ACS Photonics

pubs.acs.org/journal/apchd5

Article

Injecting Electrons into CeO_2 via Photoexcitation of Embedded Au Nanoparticles

Eleonora Spurio, Jacopo Stefano Pelli Cresi, Giuseppe Ammirati, Samuele Pelatti, Alessandra Paladini, Sergio D'Addato, Stefano Turchini, Patrick O'Keeffe, Daniele Catone, and Paola Luches*

Cite This: *ACS Photonics* 2023, 10, 1566–1574

Read Online

ACCESS | Metrics & More | Article Recommendations | Supporting Information

ABSTRACT: The electron injection efficiency and the steady state absorptance at different photon energies for a composite system made of Au NPs embedded in a cerium oxide matrix are reported. Cerium oxide can be coupled with plasmonic nanoparticles (NPs) to improve its catalytic properties by visible-light absorption. The present work is a study of the ultrafast dynamics of excited states induced by ultraviolet and visible-light excitation in Au NPs combined with cerium oxide, aimed at understanding the excitation pathways. The data, obtained by femtosecond transient absorption spectroscopy, show that the excitation of localized surface plasmon resonances (LSPRs) in the Au NPs leads to an ultrafast injection of electrons into the empty 4f states of the surrounding cerium oxide. Within the first few picoseconds, the injected electrons couple with the lattice distortion forming a polaronic excited state, with similar properties to that formed after direct band gap excitation of the oxide. At sub-picosecond delay times, we observed relevant differences in the energetics and the time dynamics as compared to the case of band gap excitation of the oxide. Using different pump energies across the LSPR-related absorption band, the efficiency of the electron injection from the NPs into the oxide was found to be rather high, with a maximum above 30%. The injection efficiency has a different trend in energy as compared to the LSPR-related static optical absorptance, showing a significant decrease in low energies. This behavior is explained considering different deexcitation pathways with variable weight across the LSPR band. The results are important for the design of materials with high overall solar catalytic efficiency.

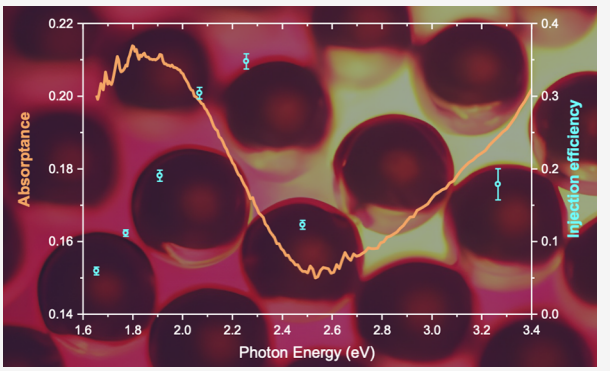

KEYWORDS: *cerium oxide, metal nanoparticles, femtosecond transient absorption spectroscopy, localized surface plasmon resonances*

INTRODUCTION

In recent years, concern for global warming has driven intense research activities toward the study of materials suitable to act as active catalysts for environmental protection, green fuel synthesis, and sustainable energy conversion. Oxides represent abundant and stable materials largely applied to convert solar to chemical energy via various photocatalytic reactions. The optimization of the materials and of their functionality requires a detailed description of the elementary processes that underlie the energy conversion processes, namely, light absorption, charge carrier generation and transport, interaction of reactants with the catalyst surface, and generation of products.[1]

Thanks to its high reducibility, cerium oxide (CeO_2) is a very important catalytic material,[2] but its efficiency as a solar photocatalysts is limited by its band gap in the ultraviolet range.[3] Different strategies can be applied to sensitize CeO_2 to visible radiation, such as doping,[4] nanostructuring,[5] and coupling with plasmonic nanoparticles (NPs), like Au, Ag, or Cu.[6−8] The latter composite systems take advantage of the large absorption and scattering cross section in the visible range, typical of plasmonic NPs. The strong interaction with the incoming radiation triggers localized surface plasmon resonances (LSPRs) in the NPs, i.e., collective resonant excitations of charges, which can relax through energy or charge transfer from the NPs to the surrounding oxide.[9,10] Different competing mechanisms are involved in the deexcitation of LSPRs and in the activation of the nearby semiconducting oxide. In general, LSPRs decay via the generation of charges with a broad energy distribution, some of which can be injected over the Schottky barrier toward the surrounding oxide. The process competes with a second mechanism in which the LSPR energy directly excites charge carriers into empty conduction band states in the oxide across the interface, leaving positive charges in the metal valence band.[9,11,12] These two mechanisms are expected to involve

Received: February 9, 2023
Revised: April 18, 2023
Accepted: April 19, 2023
Published: May 3, 2023

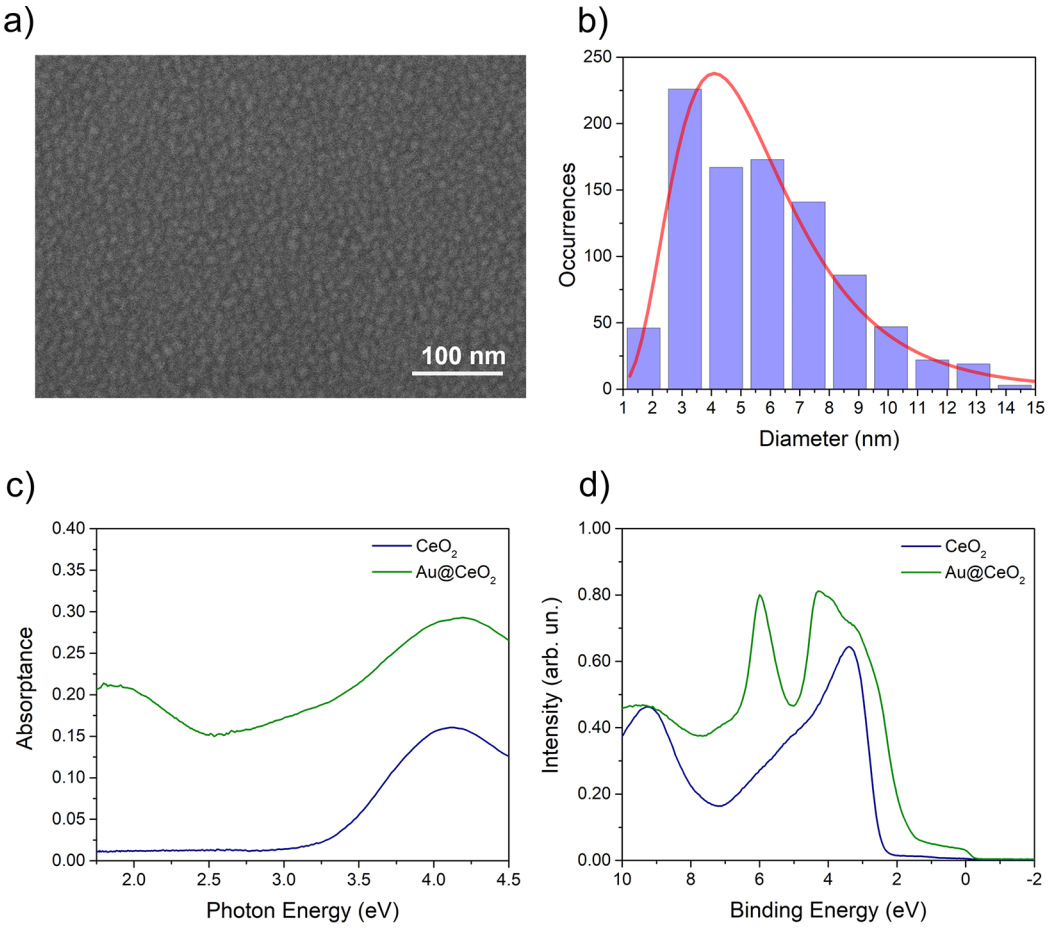

Figure 1. (a) SEM image of Au NPs on a CeO_2 film and (b) size distribution extracted from the SEM images. (c) Static optical absorptance of a CeO_2 film (blue line) and of the Au@CeO_2 sample (green line). (d) UPS spectrum of a CeO_2 film before (blue line) and after (green line) the growth of Au NPs.

different timescales as the direct injection occurs within the first tens of femtoseconds after LSPR excitation, i.e., on the timescale of dephasing of the plasmon, while the hot electron indirect injection requires a few hundreds of femtoseconds as it must occur before the hot electrons cool by electron−electron scattering.[10] On the picosecond timescale, electron−phonon scattering, leading to local thermal activation of the catalyst, prevails.[10] The processes and their efficiency strongly depend on different variables, including the energy alignment of filled and empty bands of the two materials, the height and width of the Schottky barrier between them, and the NP size, shape and density.

An experimental assessment of the processes that follow LSPR excitation in materials, which combine plasmonic NPs and oxides, is presently quite challenging because the possible deexcitation pathways are quite complex and often superposed in space and time. However, efforts in this direction can drive the optimization of photocatalysts based on such materials. Several studies have revealed an enhanced activity in photocatalysts incorporating plasmonic NPs,[8,10,13−16] but only a limited number have tried to isolate the different activation mechanisms based on the dynamics of excited states.[9,13,17] In a previous study on CeO_2 coupled with Ag NPs using femtosecond transient absorption spectroscopy (FTAS), we have identified an efficient and persistent plasmon-mediated electron injection from the Ag NPs to cerium oxide.[6] However, in the case of Ag NPs, the investigation of the electron injection dynamics at ultrashort timescales was hindered by the superposition between a photoinduced absorption (PIA) signal, characteristic of CeO_2 excitation, and the plasmon-related transient absorption (TA) signal. An element-specific analysis of the process using free-electron laser based pump-probe X-ray absorption spectroscopy allowed us to unambiguously identify a reduction of CeO_2 compatible with a plasmon-mediated transfer of electrons into Ce 4f levels and to estimate an upper limit of 200 fs for the injection time,[18] a value short enough to exclude thermal effects. Time-resolved photoemission spectroscopy was used to investigate the lifetimes of the photogenerated holes in the same system, finding a value of 100 ps for band gap excitation and of 300 ps in the case of LSPR excitation.[19] The LSPR-related TA band in Ag NPs is partially overlapped with the TA signal related to electron injection, so an analysis of the injection dynamics was not possible.[6] Since the LSPR-related TA band in Au NPs is centered at a lower energy as compared to Ag NPs, the TA signal related to electron injection could be clearly separated from the LSPR-related signal, allowing us to investigate the injection dynamics. Cu NPs show an LSPR band at a comparable energy to Au NPs; however, the interface between Cu NPs and cerium oxide is expected to be significantly less ideal than in the case of non-reactive Au NPs. For these reasons, the present work is focused on Au NPs combined with CeO_2, a system that allowed us to obtain previously unavailable information on the dynamics of injected electrons

https://doi.org/10.1021/acsphotonics.3c00184
ACS Photonics 2023, 10, 1566−1574

at ultrashort times after LSPR excitation. Moreover, the injection efficiency across the LSPR absorption band has been found to have a different trend with excitation energy as compared to the static optical absorptance.

RESULTS AND DISCUSSION

The samples for the present study were grown by molecular beam epitaxy as described in refs 20 and 21 (see the Methods section).

Scanning electron microscopy (SEM) was used to characterize the morphology of the Au NPs. Figure 1a reports a representative SEM image of Au NPs on a 2 nm CeO_2 film, showing that the Au NPs have a rather irregular shape. The Au NP size distribution is reported in Figure 1b, which shows a maximum at ∼5 nm and a full width at half-maximum (FWHM) of ∼4 nm.

Figure 1c shows the UV−vis optical absorptance of Au NPs embedded within two CeO_2 films, each 2 nm thick, hereafter referred to as Au@CeO_2, compared with a reference CeO_2 film of 4 nm thickness. The absorptance of pure CeO_2 exhibits a strong increase in the ultraviolet region, peaked around 4.1 eV, and a very small intensity in the visible range, in agreement with previous measurements of CeO_2 films grown in the same conditions[6,22] (see also the sketch in Figure 2). The incorporation of Au NPs into the oxide significantly modifies the optical absorptance of the material, with a broad band, peaked at ∼1.9 eV, appearing in the visible region due to the excitation of LSPR in Au NPs.[23,24] The width of the observed LSPR-related band is consistent with the irregular shapes of the self-assembled NPs as measured by SEM (see Figure 1a,b and the Supporting Information, Figure S3). The absorptance also shows an increase between 2.5 and 3.2 eV, due to the excitation of interband transitions in the Au NPs.[25,26] The excitation of sub-band gap defect states in the oxide, possibly present in the topmost CeO_2 film above the Au NP, can also contribute to absorptance in this region. Figure 1d shows the ultraviolet photoemission spectroscopy (UPS) spectra of a 2 nm CeO_2 film before and after Au NP deposition. The spectrum of the CeO_2 thin film (blue line) presents a dominant feature between 2 and 7 eV due to the valence band with O 2p character. The deposition of Au NPs modifies the UPS spectrum, introducing a peak at ∼6 eV binding energy and a double peak between 2 and 5 eV binding energy, related to the Au 5d band, and a non-negligible intensity up to the Fermi edge, due to the 6s band, in analogy with bulk Au[27] (see also the sketch in Figure 2).

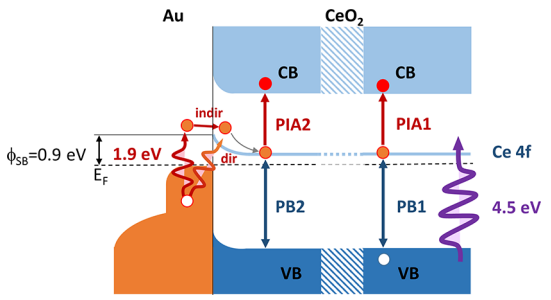

Figure 2. Sketch of the bands at the Au@CeO_2 interface. The processes induced by band gap excitation (pump at 4.5 eV) and LSPR excitation (pump at 1.9 eV) and the corresponding PIA and PB signals are schematically shown.

Figure 3 shows the false-color maps of the TA spectra of the Au@CeO_2 sample, excited with a pump at 4.5 eV, above the CeO_2 band gap (Figure 3a) and below the band gap at the LSPR of the embedded Au NPs (1.9 eV; Figure 3c), with a probe in the UV range and a delay time range limited to 0−10 ps. The maps in the full delay time range used (−1 to 300 ps) acquired with the UV and vis probe are reported in the Supporting Information, Figure S4. Figure 2b,d reports TA spectra at selected time delays. The energy and the intensity of the transient features observed and their temporal evolution provide information on the dynamics of the photoexcited states in the investigated material. For both pump energies, it is possible to clearly identify two main features in the map, one with a positive and one with a negative intensity. The positive features, labeled in Figure 2 as PIA1 and PIA2 for pump energies of 4.5 and 1.9 eV, respectively, appear at a photon energy of ∼3.5 eV, while the negative features, namely, the photoinduced bleaching (PB) and labeled as PB1 and PB2, appear at a higher energy of ∼4.1 eV. To explain the origin of PIA1 and PB1, we refer to Figure 2, which reports a sketch of the filled and empty levels at the interface between CeO_2 and Au NPs, the energies of which are based on literature density functional theory (DFT) results,[28] as well as on the UPS spectra shown in Figure 1d. CeO_2 is an n-type semiconductor with a valence band (VB) with a predominantly O 2p character and a conduction band (CB) with a predominantly Ce 5d character. The energy difference between the top of the VB and the bottom of the CB is approximately 6 eV. The material is characterized by the presence of localized empty Ce 4f states between the VB and the CB that result in an optical band gap at about 4 eV.[22] Based on previous studies on pure CeO_2[22] and on the same system coupled with Ag NPs,[6] the PIA1 feature at 3.5 eV is ascribed to photoinduced absorption of VB electrons excited by the pump into empty Ce 4f levels and subsequently reexcited by the probe into the CB of Ce 5d character (Figure 2). In analogy, the PB1 feature at 4.1 eV, corresponding to the maximum of the CeO_2 optical absorptance, as shown in Figure 1b, is ascribed to photoinduced bleaching of the VB due to an increase in the density of occupied 4f final states and to a decrease in the initial density of occupied states in the VB, as compared to the unperturbed state. The PB2 and PIA2 features in Figure 3c, acquired with an excitation energy below the band gap of CeO_2 and resonant with the Au NPs LSPR (1.9 eV), appear at approximately the same energy as PB1 and PIA1, respectively. To understand the origin of such features, the electronic band structure of Au at the interface with CeO_2 has to be considered (see the sketch in Figure 2). The density of states of the Au NPs investigated here, as shown by the UPS measurements reported in Figure 1d, is not very different from that of bulk Au, having a relatively low intensity 6s band extending within the first 2 eV below the Fermi level and a more intense 5d band with an onset at a binding energy of ∼2 eV. The alignment between metal and oxide energy levels at the interface critically depends on the interface properties and on possible charge transfers between the two materials. In the literature, Au NPs grown on CeO_2 have shown a negligible steady state charge transfer,[29] a result that is confirmed also by DFT calculations,[30] in contrast to the case of Ag[21] or Pt NPs[32] in which electrons are transferred from the metal to cerium oxide when they come into contact. The empty Ce 4f levels are very close to the Fermi level, and thus, an upward band bending of the oxide CB and VB is expected at the interface with Au.[7] The Schottky barrier, ϕ_{SB} in Figure 2, between the

https://doi.org/10.1021/acsphotonics.3c00184
ACS Photonics 2023, 10, 1566−1574

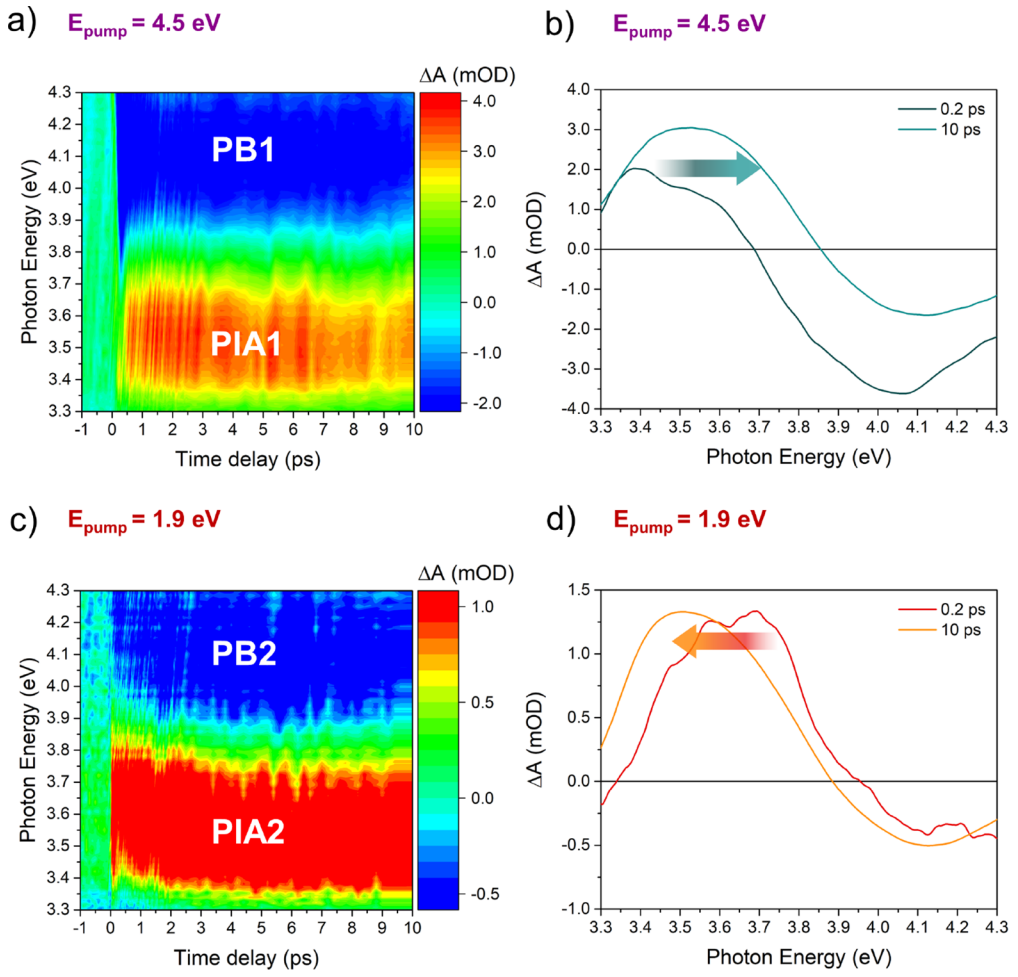

Figure 3. False-color map of the TA spectra of the Au@CeO_2 sample excited with pumps at (a) 4.5 eV (above the CeO_2 band gap) and (c) 1.9 eV (below the band gap). The PIA signals at ∼3.5 eV and the PB signals at ∼4.1 eV are indicated. (b, d) TA spectra at selected delay times of 0.2 and 10 ps for the two pump energies.

metal and the oxide is approximately 0.9 eV.[31] The LSPR, excited in the Au NPs by the pump at 1.9 eV, can decay via the generation of hot electrons with an energy distribution, which extends up to the value used for LSPR excitation (1.9 eV). The most energetic electrons have enough energy to be transferred over the approximately 0.9 eV high Schottky barrier by indirect transfer (path indicated as indir in Figure 2). Alternatively, the LSPR can decay by a direct plasmonic coupling across the chemical interface[11] in which the net effect is a transfer of electrons from the Au VB to the Ce 4f levels (path indicated as dir in Figure 2). Both the PIA2 and the PB2 signals can be assigned to the transient occupation of Ce 4f levels caused by LSPR-mediated electron injection from the NPs to the semiconductor. While the PIA2 results from the excitation of the electrons injected into the 4f states to the CB, the PB2 signal is generated by the lower density of empty final states available for the VB to 4f transition, as compared to the unperturbed state (Figure 2). We note that the intensity of the TA features observed after LSPR excitation is expectedly lower than in the case of band gap excitation due to the lower efficiency of the LSPR-mediated charge transfer process as compared to direct band gap excitation.

Before discussing the details of the time dependence of the transient signals, we focus on their spectral shapes at long time delays, when the systems have relaxed for hundreds of picoseconds after photoexcitation. In Figure 4, the comparison of the normalized transient signals averaged over 200−300 ps time delays is shown, following excitation of (i) CeO_2 at 4.5 eV

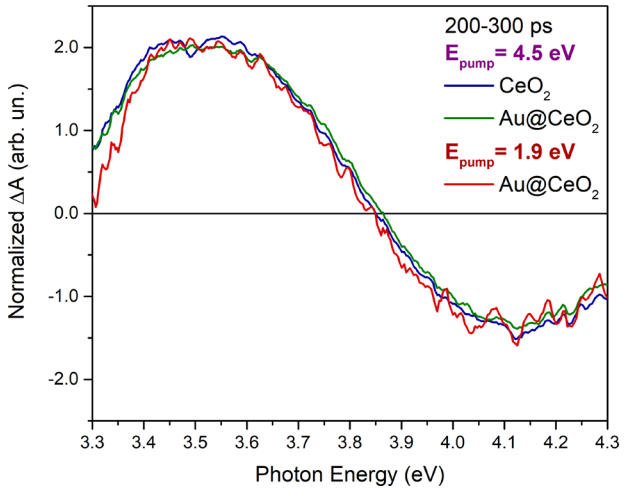

Figure 4. Normalized TA spectra averaged over 200−300 ps of Au@CeO_2 (green line) and CeO_2 (blue line) samples excited with a pump at 4.5 eV (above the CeO_2 band gap) and of the Au@CeO_2 sample excited with a pump at 1.9 eV (red line).

https://doi.org/10.1021/acsphotonics.3c00184
ACS Photonics 2023, 10, 1566−1574

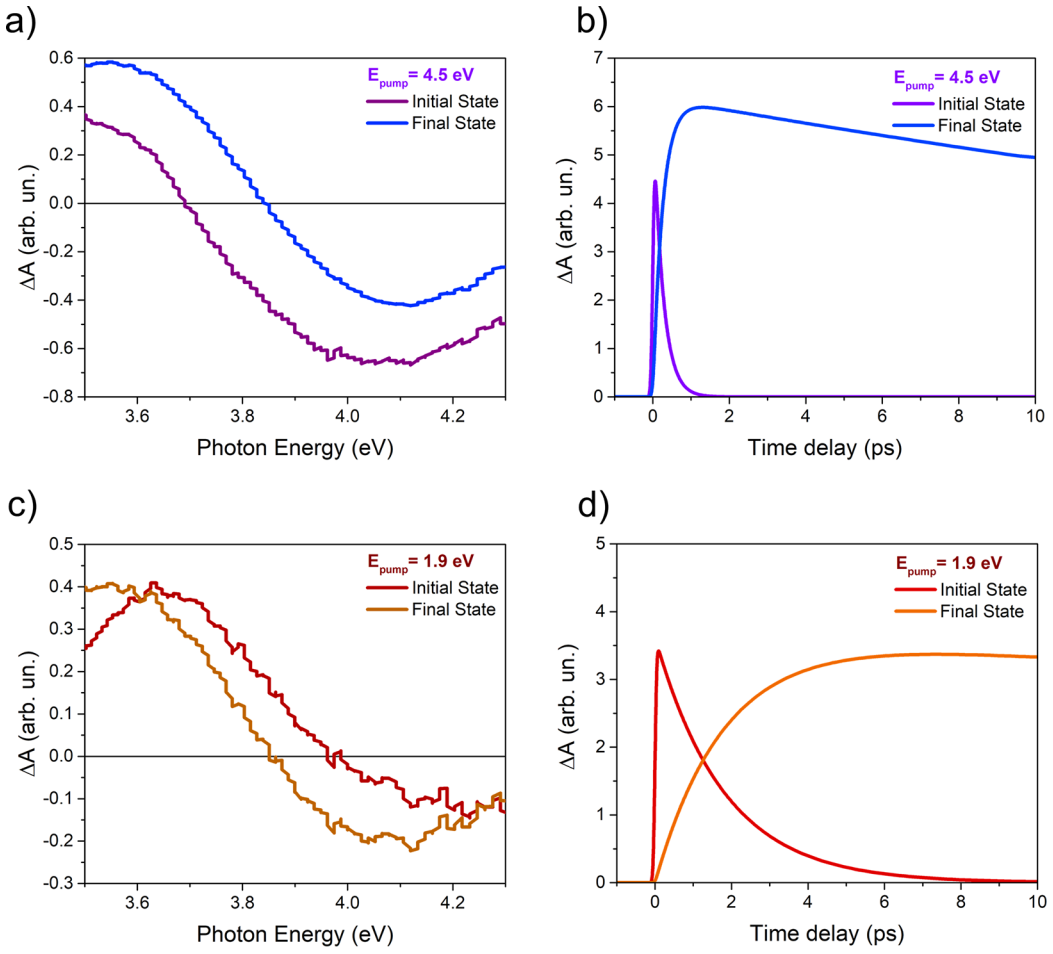

Figure 5. (a) Spectral components obtained from the global analysis for the pump at 4.5 eV; (b) weight dynamics of the two spectral components in panel (a); (c, d) same as panels (a, b) for the pump at 1.9 eV.

(blue line), (ii) Au@CeO_2 at 4.5 eV (green line), and (iii) Au@CeO_2 at 1.9 eV (red line), revealing the same spectral responses in the three cases. This shows that the intermediate excited states reached by the Au@CeO_2 system within a few hundreds of picoseconds are the same for the two pump energies used. Moreover, it has the same spectral shape as that obtained on a pure CeO_2 sample excited above the band gap. Based on the analysis presented in ref 22, which shows that the above band gap photoexcitation in a pure cerium oxide results in the formation of a small polaron in the excited state, we conclude that both the above gap and LSPR excitation in the Au@CeO_2 system result in the formation of a small polaron in analogy with pure CeO_2. This hypothesis is also consistent with the kinetic behavior of the PIA1, PIA2, PB1, and PB2 signals, which show a non-negligible intensity at all delay times investigated, in close analogy with CeO_2[24] and Ag@CeO_2,[6] because of the relatively long recombination times of photoexcited carriers in the oxide. Therefore, Au NPs do not introduce different recombination channels within the investigated delay time range.

To analyze the kinetics of the TA signals in detail, we used a global analysis approach (CarpetView software package) that allowed us to extract the transient photoexcited components from the TA spectra with their temporal evolution. As shown in Figure 3b,d, the TA spectra show non-negligible modifications in energy and intensity within the first few picoseconds after excitation for both pump energies. Following the approach used in ref 22, the temporal evolution of the spectra was modeled using two components, an initially photoexcited state and a long living final state. The shape and the exponential decay/rise constants of the two components are left as free fitting parameters. The components obtained using this approach and the sequential exponential dynamics of their intensity for the two pump energies are shown in Figure 5. In analogy with the case of pure ceria[22] for the pump at 4.5 eV, the two components are interpreted as being due to the initially populated excited 4f states that relax into a polaronic state at lower energy, resulting in a higher energy PIA (see the arrow in Figure 3b and Figure 5a). In this model, the PB remains at the same energy, although it may appear to shift due to the overlap with the PIA. As shown in Figure 5b, for the pump above the band gap, the initial state decays into the final state within the first picosecond. Overall, the dynamics of the excited states of the Au@CeO_2 system pumped above the band gap shows the same trend as that of bare ceria,[22] consistent with the expected negligible modifications induced by the presence of Au NPs on the electronic structure of the ceria matrix. The situation is significantly different in the case of plasmonic excitation of the Au@CeO_2 system shown in Figure 5c, in which the PIA is initially at a higher energy than in the final state, contrary to what was observed in the case of excitation above the ceria gap (see the arrow in Figure 3d). As shown in Figure 5d, in this case, the time required to evolve from the initial to the final state is longer (more than 4 ps)

https://doi.org/10.1021/acsphotonics.3c00184
ACS Photonics 2023, 10, 1566−1574

than for the above band gap excitation (~1 ps). Both of the LSPR-mediated injection processes (dir and indir) occur on a much faster timescale; for example, the Ag@CeO_2 system showed a time constant shorter than 200 fs.[18] Furthermore, the polaron state is also known to form with a time constant of approximately 300 fs after photoexcitation above the band gap.[22] Therefore, the energetic and temporal dynamics observed here cannot be assigned to any of these processes. A possible explanation may lie in the fact that the electrons are injected into interface states, the energy of which may lead to a different energy position of the PIA maximum with respect to bulk states. The hypothesis that the intermediate occupied 4f states decrease in energy more slowly than the final 5d CB states as the excited state propagates from the interface (see also the sketch in Figure 2) is consistent with the observed overall reduction of the transition energy of the PIA at ultrashort decay times and with the longer time required to evolve into the bulk-like polaronic state, which dominates the TA spectra at long delay times.

Having demonstrated that after LSPR excitation in Au NPs, an injection of electrons to CeO_2 actually occurs and that it leads to an excited state comparable to that populated by the above band gap excitation within a few hundreds of picoseconds, we now estimate the efficiency of the process across the LSPR absorption band. Since the PIA signal intensity at sub-band gap energies is proportional to the density of electrons in the Ce 4f levels after the excitation, the injection efficiency can be quantified by comparing the intensity of the PIA signal of the Au@CeO_2 sample pumped at different pump energies with the intensity of the same signal of the sample pumped at 4.5 eV. Following the procedure reported in refs 6 and 24 under the assumption that each absorbed photon with energy higher than the CeO_2 band gap excites an electron from the valence band to Ce 4f levels, the absorbed photon density is

$$n_{ph} = \frac{A(\omega_{pump})\cdot\Phi}{E_{pump}\cdot D}$$

where $A(\omega_{pump})$ is the absorptance of the sample at the pump frequency evaluated from Figure 1c, Φ is the pump fluence, E_{pump} is the pump energy, and D is the total sample thickness.

The absorbed photon density can be correlated to the density of electrons excited in the Ce 4f levels, estimated by the integral of the intensity of the PIA signal between 50 and 250 ps. The short delay time range was not considered because the shape of the signals is affected by different shifts in energy at the different pump energies. The proportionality constant κ between the integral intensity of the PIA signal and n_{ph} was obtained as the ratio between these two quantities. The ratio between the κ values of Au@CeO_2 pumped at the different energies with the reference κ measured on Au@CeO_2 pumped at 4.5 eV corresponds to the charge injection efficiency from the Au NPs to CeO_2 (see the Supporting Information for details).

Figure 6 presents the electron injection efficiencies, estimated following the method described above, together with the optical absorptance of Au@CeO_2 in the same energy region. At a pump energy of 3.3 eV, an electron injection efficiency of 18 ± 2% is assigned to the interband excitation in the Au NPs followed by an indirect injection of the resulting hot electrons over the Schottky barrier between Au and CeO_2 (approximately 0.9 eV[31]) into the CeO_2 CB (Figures 1d and 3). The electron injection efficiency drastically increases above 35 ± 1% at 2.25 eV, an energy that excites the high energy wing of the LSPR of the Au NPs, and it gradually decreases at lower pump energies, reaching a value below 10% at 1.6 eV, showing a trend that does not follow the intensity of the LSPR absorptance. Indeed, the indirect injection is expected to decrease its efficiency as the photon energy is decreased. The observed non-monotonic trend of the injection efficiency with energy may be due to the additional action of the LSPR-mediated direct mechanism (see also Figure 2) that enhances the electron injection in the 1.90−2.25 eV energy range, while at lower pump energies, the reduced efficiency is due to the lower probability to inject excited electrons into the semiconductor.

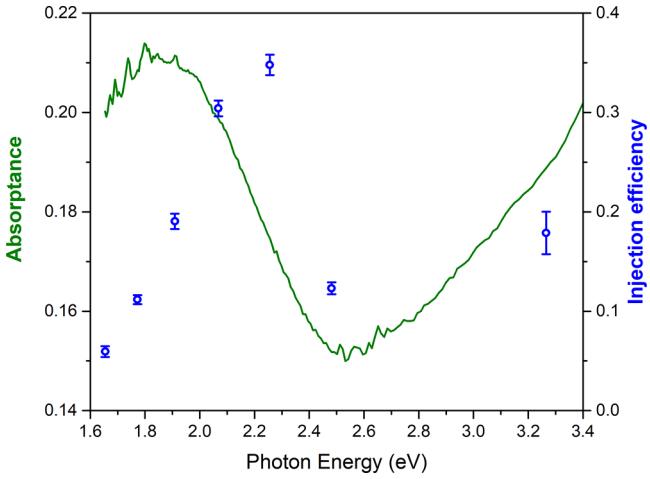

Figure 6. Electron injection efficiency (blue circles) as a function of the pump energy. The steady state optical absorptance (green curve) is also reported for comparison.

We note that a mismatch between the injection efficiency and the intensity of the LSPR resonance was observed also in the case of Au NPs coupled with TiO_2[24,32] and for Ag NPs coupled with cerium oxide.[6] As CeO_2 is a reducible oxide, the efficient charge transfer induced by visible-light absorption is expected to have a relevant effect on the oxide catalytic properties. The presence of extra charge in the 4f states is in fact predicted to decrease the oxygen vacancy formation energy and in turn to increase the redox activity. The low recombination rate of the excited charge within times of the order of hundreds of picoseconds is in agreement with the hole lifetimes observed on the similar system made of Ag NPs[33] on CeO_2.[19] We emphasize that this aspect is very promising in the view of obtaining an efficient photocatalytic material, in which the plasmon-induced thermal activation, expected to take place in a nanosecond time regime, can be enhanced by favorable persistent electronic modifications. Further conclusions of this work are that interband transitions in gold are less efficient at transferring charge to the ceria than LSPR-mediated excitations and that increasing the overlap of the LSPR with the solar spectrum at lower energies will not increase the overall solar efficiency.

It has to be noted that cerium oxide combined with plasmonic Au nanoparticles finds wide applications, not only in heterogeneous photocatalysis and photoelectrochemistry, e.g., for selective oxidation of alcohols,[7,33] photodegradation of organic pollutants,[34] and photocatalytic CO_2 reduction,[35] but also in nanomedicine, as an innovative drug with combined

https://doi.org/10.1021/acsphotonics.3c00184
ACS Photonics 2023, 10, 1566−1574

antioxidant and photothermal properties.[36,37] An improved description of the processes that follow visible-light excitation is therefore beneficial in the view of an optimized design of this class of materials in various fields of application.

CONCLUSIONS

We investigated the dynamics of photoexcited states in a composite system made of Au NPs embedded within a thin film of cerium oxide. The optical absorptance of the sample presents a broad band in the visible range that is assigned to the LSPR excitation in the NPs. FTAS measurements showed that LSPR excitations in the Au NPs relax by transferring electrons to the surrounding semiconductor. At ultrashort delay times, below a few picoseconds, a markedly different energetic and temporal dynamics is observed in the case of LSRP-mediated injection as compared to direct band gap excitation. The observed differences are compatible with the expected modifications of the electronic properties at the interface between the metal NP and the oxide. Interestingly, after a few picoseconds, both the band gap and LSPR excitation lead to the same bulk-like polaronic state. By comparing the injection efficiencies following interband and LSPR excitations, we suggest that the interband injection is dominated by the indirect mechanism while the LSPR-mediated injection takes place by both direct and indirect mechanisms. The electron injection efficiency following LSPR excitation shows a maximum over 30% at 2.25 eV, an energy that does not correspond to the maximum of LSPR-related optical absorptance, suggesting that the injection efficiency does not simply follow the intensity of the plasmonic excitation.

METHODS

The samples for the present study were grown in an ultrahigh vacuum (UHV) apparatus ($P \sim 10^{-10}$ mbar), which consists of two connected UHV chambers: an evaporation chamber, equipped with evaporators and gas lines for reactive molecular beam epitaxy (MBE) growth, and a chamber equipped with facilities for substrate preparation, X-ray photoemission spectroscopy (XPS), and ultraviolet photoemission spectroscopy (UPS). The use of different substrates was necessary to apply the different characterization techniques. For UV−vis spectrophotometry and femtosecond transient absorption spectroscopy (FTAS) measurements, a quartz substrate, ensuring a good optical transparency in the visible range, was used. The sample consists of a layer of Au NPs of 2 nm nominal thickness, embedded between two CeO_2 thin films of 2 nm thickness, referred to as Au@CeO_2. A pure CeO_2 film of 4 nm thickness was also grown on quartz for reference. For morphological characterization using SEM, a Si substrate with thermal oxide was used to assure a high electric conductivity. A CeO_2 film of 2 nm thickness and a layer of Au NPs of 2 nm nominal thickness were grown on top of it. A metallic Pt(111) substrate was necessary for UPS measurements since even mild charging effects had to be avoided. The quartz and Si substrates were cleaned by a 5 min bath in acetone at 423 K and by two subsequent ultrasonic baths in acetone and in isopropanol at 353 K for 3 min each. The Pt(111) substrate was prepared by cycles of sputtering (1 keV and 1 μA) and annealing (1040 K) until the surface contamination was below the XPS detection limit. The CeO_2 thin films were grown as described in ref 20 by reactive evaporation of Ce, using an e-beam evaporator, in an oxygen partial pressure of 10^{-7} mbar. Au was evaporated from a Knudsen cell and spontaneously self-assembled into NPs, as expected for late transition metals grown by physical synthesis methods on oxide surfaces.[38] The thickness of the film and the nominal thickness of the metal, which determines the size distribution and the density of NPs,[21] were calibrated using a quartz microbalance. The sample morphology, and in particular the size, shape, and density of Au NPs on the cerium oxide film, is not expected to be significantly different on quartz and on Si with thermal oxide since the surface composition and roughness of the two substrates are very similar. Moreover, the surface of CeO_2 films grown at room temperature has a rather rough morphology even on flat single crystal metal surfaces.[20]

After the growth, all the samples were characterized by *in situ* XPS to obtain quantitative information on the deposited quantity of CeO_2 and Au and on possible variations of the chemical state of cerium oxide and of the metal (see the Supporting Information, Figure S1 for details). The spectra were acquired at normal emission using Al K_α photons from a double-anode X-ray source and a hemispherical electron analyzer. UPS using a He lamp with He I emission and a hemispherical electron analyzer at normal emission was used to assess the valence band density of states at the different stages of growth. Information on NP morphology was obtained using SEM (FEI Nova NanoSEM 450) on the sample grown on the Si substrate. The GMS3 GATAN software by DigitalMicrograph was used to obtain the Au NP size distribution.

The optical apparatus for UV−vis spectrophotometry consists of a xenon lamp, providing white non-polarized light, an ORIEL-MS257 monochromator, a polarizer, and a silicon photodetector. The absorptance A of the sample is evaluated as $A = 1 - (T + R)$, where T and R are the transmittance and the reflectance, respectively, i.e., the fraction of transmitted and reflected light, measured with the impinging photon beam forming an angle of 22° with the sample surface normal. The absorptance spectral shape was comparable for s- and p-polarized light (see the Supporting Information, Figure S2). In the present work, the spectra acquired with s-polarized light, having a higher signal-to-noise ratio, were reported.

FTAS measurements were performed using a femtosecond laser system described in detail elsewhere.[39,40] As an optical pump, a laser pulse generated by an optical parametric amplifier was tuned either to an energy above the band gap of ceria or to energies in the visible range across the plasmonic resonance of the embedded Au NPs. For the probe, a small portion of the fundamental (approximately 3 μJ) was passed through a BBO crystal to generate the second harmonic (400 nm) that was focused into a rotating CaF_2 crystal to generate a supercontinuum in the UV energy range (3.50−4.35 eV). The temporal delay of the probe pulse was varied between −1 and 300 ps by varying the length of the optical path of the beam used to generate the white light. In the TA maps presented in this work, the chirp of the probe pulse was corrected. The instrument response function (IRF) was evaluated in separate experiments to be Gaussian with a FHWM of 70 fs. The pump fluences were 0.7 mJ/cm^2 for the 4.5 and 3.3 eV energies and 1 mJ/cm^2 for the other pump energies, which is sufficiently low not to induce melting of the nanoparticles.[41]

https://doi.org/10.1021/acsphotonics.3c00184
ACS Photonics 2023, 10, 1566−1574

■ ASSOCIATED CONTENT

Supporting Information

The Supporting Information is available free of charge at https://pubs.acs.org/doi/10.1021/acsphotonics.3c00184.

XPS analysis, aspect ratio of the Au NPs, UV−vis spectrophotometry, simulations of the polarizability of Au NPs in CeO_2, full TA maps, and evaluation of the injection efficiency (PDF)

■ AUTHOR INFORMATION

Corresponding Author

Paola Luches − *Istituto Nanoscienze, CNR (NANO-CNR), 41125 Modena, Italy;* orcid.org/0000-0003-1310-5357; Email: paola.luches@nano.cnr.it

Authors

Eleonora Spurio − *Dipartimento FIM, Università degli Studi di Modena e Reggio Emilia, 41125 Modena, Italy; Istituto Nanoscienze, CNR (NANO-CNR), 41125 Modena, Italy*

Jacopo Stefano Pelli Cresi − *Elettra-Sincrotrone Trieste, 34012 Trieste, Italy*

Giuseppe Ammirati − *CHOSE (Centre for Hybrid and Organic Solar Energy), Department of Electronic Engineering, University of Rome Tor Vergata, 00133 Rome, Italy; Istituto di Struttura della Materia − CNR (ISM-CNR), EuroFEL Support Laboratory (EFSL), 00133 Rome, Italy*

Samuele Pelatti − *Dipartimento FIM, Università degli Studi di Modena e Reggio Emilia, 41125 Modena, Italy; Istituto Nanoscienze, CNR (NANO-CNR), 41125 Modena, Italy*

Alessandra Paladini − *Istituto di Struttura della Materia − CNR (ISM-CNR), EuroFEL Support Laboratory (EFSL), Monterotondo Scalo 00015, Italy*

Sergio D'Addato − *Dipartimento FIM, Università degli Studi di Modena e Reggio Emilia, 41125 Modena, Italy; Istituto Nanoscienze, CNR (NANO-CNR), 41125 Modena, Italy*

Stefano Turchini − *Istituto di Struttura della Materia − CNR (ISM-CNR), EuroFEL Support Laboratory (EFSL), 00133 Rome, Italy*

Patrick O'Keeffe − *Istituto di Struttura della Materia − CNR (ISM-CNR), EuroFEL Support Laboratory (EFSL), Monterotondo Scalo 00015, Italy;* orcid.org/0000-0002-8676-4436

Daniele Catone − *Istituto di Struttura della Materia − CNR (ISM-CNR), EuroFEL Support Laboratory (EFSL), 00133 Rome, Italy;* orcid.org/0000-0002-7649-2756

Complete contact information is available at: https://pubs.acs.org/10.1021/acsphotonics.3c00184

Funding

This work was financed by the European Union - NextGenerationEU (National Sustainable Mobility Center CN00000023, Italian Ministry of University and Research Decree no. 1033, 17/06/2022, Spoke 11, Innovative Materials & Lightweighting). The opinions expressed are those of the authors only and should not be considered as representative of the European Union or the European Commission's official position. Neither the European Union nor the European Commission can be held responsible for them.

Notes

The authors declare no competing financial interest.

■ REFERENCES

(1) Takanabe, K. Photocatalytic Water Splitting: Quantitative Approaches toward Photocatalyst by Design. *ACS Catal.* **2017**, *7*, 8006−8022.

(2) Montini, T.; Melchionna, M.; Monai, M.; Fornasiero, P. Fundamentals and Catalytic Applications of CeO2-Based Materials. *Chem. Rev.* **2016**, *116*, 5987−6041.

(3) Vangelista, S.; Piagge, R.; Ek, S.; Sarnet, T.; Ghidini, G.; Martella, C.; Lamperti, A. Structural, chemical and optical properties of cerium dioxide film prepared by atomic layer deposition on TiN and Si substrates. *Thin Solid Films* **2017**, *636*, 78−84.

(4) Wu, T. S.; Chen, Y. W.; Weng, S. C.; Lin, C. N.; Lai, C. H.; Huang, Y. J.; Jeng, H. T.; Chang, S. L.; Soo, Y. L. Dramatic band gap reduction incurred by dopant coordination rearrangement in Co-doped nanocrystals of CeO2. *Sci. Rep.* **2017**, *7*, 4715.

(5) Thill, A. S.; Lobato, F. O.; Vaz, M. O.; Fernandes, W. P.; Carvalho, V. E.; Soares, E. A.; Poletto, F.; Teixeira, S. R.; Bernardi, F. Shifting the band gap from UV to visible region in cerium oxide nanoparticles. *Appl. Surf. Sci.* **2020**, *528*, No. 146860.

(6) Pelli Cresi, J. S.; Spadaro, M. C.; D'Addato, S.; Valeri, S.; Benedetti, S.; Di Bona, A.; Catone, D.; Di Mario, L.; O'Keeffe, P.; Paladini, A.; Bertoni, G.; Luches, P. Highly efficient plasmon-mediated electron injection into cerium oxide from embedded silver nanoparticles. *Nanoscale* **2019**, *11*, 10282−10291.

(7) Li, B.; Gu, T.; Ming, T.; Wang, J.; Wang, P.; Wang, J.; Yu, J. C. (Gold Core)@(Ceria Shell) Nanostructures for Plasmon-Enhanced Catalytic Reactions under Visible Light. *ACS Nano* **2014**, *8*, 8152−8162.

(8) Kim, S. M.; Lee, H.; Goddeti, K. C.; Kim, S. H.; Park, J. Y. Photon-Induced Hot Electron Effect on the Catalytic Activity of Ceria-Supported Gold Nanoparticles. *J. Phys. Chem. C* **2015**, *119*, 16020−16025.

(9) Wu, N. Plasmonic metal-semiconductor photocatalysts and photoelectrochemical cells: a review. *Nanoscale* **2018**, *10*, 2679−2696.

(10) Zhang, Y.; He, S.; Guo, W.; Hu, Y.; Huang, J.; Mulcahy, J. R.; Wei, W. D. Surface-Plasmon-Driven Hot Electron Photochemistry. *Chem. Rev.* **2018**, *118*, 2927−2954.

(11) Tan, S.; Argondizzo, A.; Ren, J.; Liu, L.; Zhao, J.; Petek, H. Plasmonic coupling at a metal/semiconductor interface. *Nat. Photonics* **2017**, *11*, 806−812.

(12) Wu, K.; Chen, J.; McBride, J. R.; Lian, T. Efficient hot-electron transfer by a plasmon-induced interfacial charge-transfer transition. *Science* **2015**, *349*, 632.

(13) Linic, S.; Christopher, P.; Ingram, D. B. Plasmonic-metal nanostructures for efficient conversion of solar to chemical energy. *Nat. Mater.* **2011**, *10*, 911−921.

(14) Hou, W.; Hung, W. H.; Pavaskar, P.; Goeppert, A.; Aykol, M.; Cronin, S. B. Photocatalytic Conversion of CO2 to Hydrocarbon Fuels via Plasmon-Enhanced Absorption and Metallic Interband Transitions. *ACS Catal.* **2011**, *1*, 929−936.

(15) Mukherjee, S.; Libisch, F.; Large, N.; Neumann, O.; Brown, L. V.; Cheng, J.; Lassiter, J. B.; Carter, E. A.; Nordlander, P.; Halas, N. J. Hot Electrons Do the Impossible: Plasmon-Induced Dissociation of H2 on Au. *Nano Lett.* **2013**, *13*, 240−247.

(16) Pan, J.; Zhang, L.; Zhang, S.; Shi, Z.; Wang, X.; Song, S.; Zhang, H. Half-Encapsulated Au Nanorods@CeO2 Core@Shell Nanostructures for Near-Infrared Plasmon-Enhanced Catalysis. *ACS Appl. Nano Mater.* **2019**, *2*, 1516−1524.

(17) Tang, H.; Chen, C.-J.; Huang, Z.; Bright, J.; Meng, G.; Liu, R.-S.; Wu, N. Plasmonic hot electrons for sensing, photodetection, and solar energy applications: A perspective. *J. Chem. Phys.* **2020**, *152*, No. 220901.

(18) Pelli Cresi, J. S.; Principi, E.; Spurio, E.; Catone, D.; O'Keeffe, P.; Turchini, S.; Benedetti, S.; Vikatakavi, A.; D'Addato, S.; Mincigrucci, R.; Foglia, L.; Kurdi, G.; Nikolov, I. P.; De Ninno, G.; Masciovecchio, C.; Nannarone, S.; Kopula Kesavan, J.; Boscherini, F.; Luches, P. Ultrafast Dynamics of Plasmon-Mediated Charge Transfer in Ag@CeO2 Studied by Free Electron Laser Time-Resolved X-ray Absorption Spectroscopy. *Nano Lett.* **2021**, *21*, 1729−1734.

(19) Pelli Cresi, J. S.; Spurio, E.; Di Mario, L.; O'Keeffe, P.; Turchini, S.; Benedetti, S.; Pierantozzi, G. M.; De Vita, A.; Cucini, R.; Catone, D.; Luches, P. Lifetime of Photogenerated Positive Charges in Hybrid Cerium Oxide-Based Materials from Space and Mirror Charge Effects in Time-Resolved Photoemission Spectroscopy. *J. Phys. Chem. C* **2022**, *126*, 11174−11181.
(20) Luches, P.; Pagliuca, F.; Valeri, S. Morphology, Stoichiometry, and Interface Structure of CeO_2 Ultrathin Films on Pt(111). *J. Phys. Chem. C* **2011**, *115*, 10718−10726.
(21) Luches, P.; Pagliuca, F.; Valeri, S.; Illas, F.; Preda, G.; Pacchioni, G. Nature of Ag Islands and Nanoparticles on the CeO2(111) Surface. *J. Phys. Chem. C* **2012**, *116*, 1122−1132.
(22) Pelli Cresi, J. S.; Di Mario, L.; Catone, D.; Martelli, F.; Paladini, A.; Turchini, S.; D'Addato, S.; Luches, P.; O'Keeffe, P. Ultrafast Formation of Small Polarons and the Optical Gap in CeO2. *J. Phys. Chem. Lett.* **2020**, *11*, 5686−5691.
(23) Furube, A.; Du, L.; Hara, K.; Katoh, R.; Tachiya, M. Ultrafast Plasmon-Induced Electron Transfer from Gold Nanodots into TiO2 Nanoparticles. *J. Am. Chem. Soc.* **2007**, *129*, 14852−14853.
(24) Ratchford, D. C.; Dunkelberger, A. D.; Vurgaftman, I.; Owrutsky, J. C.; Pehrsson, P. E. Quantification of Efficient Plasmonic Hot-Electron Injection in Gold Nanoparticle−TiO2 Films. *Nano Lett.* **2017**, *17*, 6047−6055.
(25) Hartland, G. V. Optical Studies of Dynamics in Noble Metal Nanostructures. *Chem. Rev.* **2011**, *111*, 3858−3887.
(26) Zhang, X.; Huang, C.; Wang, M.; Huang, P.; He, X.; Wei, Z. Transient localized surface plasmon induced by femtosecond interband excitation in gold nanoparticles. *Sci. Rep.* **2018**, *8*, 10499.
(27) Baer, D. R.; Gordon, R. L.; Hubbard, C. W. Work function and UPS study of Au and O on Re. *Appl. Surf. Sci.* **1990**, *45*, 71−83.
(28) Pan, Y.; Nilius, N.; Freund, H.-J.; Paier, J.; Penschke, C.; Sauer, J. Titration of Ce^{3+} Ions in the CeO_2(111) Surface by Au Adatoms. *Phys. Rev. Lett.* **2013**, *111*, No. 206101.
(29) Baron, M.; Bondarchuk, O.; Stacchiola, D.; Shaikhutdinov, S.; Freund, H. J. Interaction of Gold with Cerium Oxide Supports: CeO2(111) Thin Films vs CeOx Nanoparticles. *J. Phys. Chem. C* **2009**, *113*, 6042−6049.
(30) Branda, M. M.; Hernández, N. C.; Sanz, J. F.; Illas, F. Density Functional Theory Study of the Interaction of Cu, Ag, and Au Atoms with the Regular CeO2 (111) Surface. *J. Phys. Chem. C* **2010**, *114*, 1934−1941.
(31) Grosse, V.; Bechstein, R.; Schmidl, F.; Seidel, P. Conductivity and dielectric properties of thin amorphous cerium dioxide films. *J. Phys. D: Appl. Phys.* **2007**, *40*, 1146−1149.
(32) Du, L.; Furube, A.; Hara, K.; Katoh, R.; Tachiya, M. Ultrafast plasmon induced electron injection mechanism in gold−TiO2 nanoparticle system. *J. Photochem. Photobiol., C* **2013**, *15*, 21−30.
(33) Tanaka, A.; Hashimoto, K.; Kominami, H. Preparation of Au/CeO2 Exhibiting Strong Surface Plasmon Resonance Effective for Selective or Chemoselective Oxidation of Alcohols to Aldehydes or Ketones in Aqueous Suspensions under Irradiation by Green Light. *J. Am. Chem. Soc.* **2012**, *134*, 14526−14533.
(34) Khan, M. M.; Ansari, S. A.; Pradhan, D.; Han, D. H.; Lee, J.; Cho, M. H. Defect-Induced Band Gap Narrowed CeO2 Nanostructures for Visible Light Activities. *Ind. Eng. Chem. Res.* **2014**, *53*, 9754−9763.
(35) Wei, Y.; Li, X.; Zhang, Y.; Yan, Y.; Huo, P.; Wang, H. G-C3N4 quantum dots and Au nano particles co-modified CeO2/Fe3O4 micro-flowers photocatalyst for enhanced CO2 photoreduction. *Renewable Energy* **2021**, *179*, 756−765.
(36) Ge, K.; Mu, Y.; Liu, M.; Bai, Z.; Liu, Z.; Geng, D.; Gao, F. Gold Nanorods with Spatial Separation of CeO2 Deposition for Plasmonic-Enhanced Antioxidant Stress and Photothermal Therapy of Alzheimer's Disease. *ACS Appl. Mater. Interfaces* **2022**, *14*, 3662−3674.
(37) Li, Z.; Wu, X.; Gu, W.; Zhou, P.; Chen, H.; Wang, W.; Cai, Z.; Cao, S.; Guo, K.; Zheng, X.; Gao, F. Photogenerated electrons from CeO2 via upconversion of excitons to conduction band enhanced photocatalysis for Photo-Therapy of Rheumatoid arthritis. *Chem. Eng. J.* **2022**, *446*, No. 136904.
(38) Campbell, C. T. Ultrathin metal films and particles on oxide surfaces: structural, electronic and chemisorptive properties. *Surf. Sci. Rep.* **1997**, *27*, 1−111.
(39) Ferrera, M.; Della Valle, G.; Sygletou, M.; Magnozzi, M.; Catone, D.; O'Keeffe, P.; Paladini, A.; Toschi, F.; Mattera, L.; Canepa, M.; Bisio, F. Thermometric Calibration of the Ultrafast Relaxation Dynamics in Plasmonic Au Nanoparticles. *ACS Photonics* **2020**, *7*, 959−966.
(40) Catone, D.; Di Mario, L.; Martelli, F.; O'Keeffe, P.; Paladini, A.; Stefano Pelli Cresi, J.; Sivan, A. K.; Tian, L.; Toschi, F.; Turchini, S. Ultrafast optical spectroscopy of semiconducting and plasmonic nanostructures and their hybrids. *Nanotechnology* **2020**, *32*, No. 025703.
(41) Magnozzi, M.; Proietti Zaccaria, R.; Catone, D.; O'Keeffe, P.; Paladini, A.; Toschi, F.; Alabastri, A.; Canepa, M.; Bisio, F. Interband Transitions Are More Efficient Than Plasmonic Excitation in the Ultrafast Melting of Electromagnetically Coupled Au Nanoparticles. *J. Phys. Chem. C* **2019**, *123*, 16943−16950.

https://doi.org/10.1021/acsphotonics.3c00184
ACS Photonics 2023, 10, 1566−1574